nature physics

ARTICLES

PUBLISHED ONLINE: 8 DECEMBER 2013 | DOI: 10.1038/NPHYS2826

Room-temperature quantum microwave emitters based on spin defects in silicon carbide

H. Kraus[1], V. A. Soltamov[2], D. Riedel[1], S. Väth[1], F. Fuchs[1], A. Sperlich[1], P. G. Baranov[2], V. Dyakonov[1,3]* and G. V. Astakhov[1]

Atomic-scale defects in silicon carbide are always present and usually limit the performance of this material in high-power electronics and radiofrequency communication. Here, we reveal a family of homotypic silicon vacancy defects in silicon carbide exhibiting attractive spin properties. In particular, the defect spins can be initialized and read out even at room temperature by means of optically detected magnetic resonance, suggesting appealing applications such as spin qubits and spin magnetometers. Using this technique we detect two-quantum spin resonances, providing strong evidence for the $S = 3/2$ ground state of the silicon vacancy defects. The optically induced population inversion of these high-spin ground states leads to stimulated microwave emission, which we directly observed in our silicon carbide crystals. The analysis based on the experimentally obtained parameters shows that this property can be used to implement solid-state masers and extraordinarily sensitive radiofrequency amplifiers.

Quantum optical devices, such as lasers, have changed our everyday life and have become ubiquitous. Light quanta—photons—play a central role in the existing optical quantum technologies[1,2]. In contrast, control of microwave photons is much more delicate because their energy (10^{-7}–10^{-4} eV) is several orders of magnitude smaller than the energy carried by optical photons (about 1 eV). To increase the emission efficiency, the present-day quantum microwave emitters (including masers) are necessarily cooled down to cryogenic temperature[3–5]. This limits possible applications to a few niche uses. The most notable is the low-noise microwave amplification systems for deep-space communication, where high-electron-mobility transistors are not sensitive enough[6].

Non-classical room-temperature microwave emission can be achieved in a system that possesses an efficient spin pumping mechanism, creating a population inversion even at room temperature, and such a low spin relaxation rate that thermal equilibrium is not re-established during the pumping cycle. In fact, several observations of microwave emission in organic systems at room temperature have been published over the years[7–9], and the masing effect in pulsed mode has recently been achieved in an organic mixed molecular crystal[10]. Here, a population inversion is generated owing to the optical excitation followed by spin-selective relaxation to the triplet state. As, in this molecular crystal, the triplet state is an excited state, the relaxation to the singlet ground state may limit maser performance, resulting in a particular high optical pumping threshold value (several hundreds of watts). In addition, the signal processing rate for the above maser amplifier would be limited by the pulse repetition rate, which is 1 Hz. For this reason, it is necessary to achieve a steady-state stimulated emission, where the signal processing rate is given by the bandwidth, which is typically $\Delta\nu \sim 10$ MHz.

A possible candidate to fulfil these requirements is the nitrogen–vacancy (NV) defect in diamond[11]. It is well established that optical excitation facilitates efficient spin pumping of its $S = 1$ ground singlet state even at room temperature. In this system, the lower spin sublevel with $m_s = 0$ is preferentially populated in zero magnetic field[12], and inverse population is not created. This problem can potentially be overcome by applying a strong enough magnetic field, such that the Zeeman $m_s = -1$ spin sublevel becomes the lowest energy state. However, to the best of our knowledge diamond has not been considered in this respect so far.

Silicon vacancy defects

Intrinsic defects in silicon carbide (SiC) have recently revealed similar spin properties to the NV defects in diamond[13,14]. In particular, the silicon vacancy (V_{Si}) defects (Fig. 1a) have demonstrated a high potential for spintronic and photonic applications[15,16]. Room-temperature coherent spin alignment of V_{Si} has been achieved using direct-detected electron spin resonance[17] (ESR). Remarkably, this technique is based on a strong optical pulsed excitation (equivalent continuous-wave power of 250 kW and repetition rate of 11 Hz) and it is not compatible with single-spin detection. Importantly, the spin structure of V_{Si} is still the subject of long-standing debates[18–23].

In this work, we demonstrate that the V_{Si} defects can be controlled at room temperature using optically detected magnetic resonance (ODMR), a standard technique to manipulate single NV defect spins[11]. Using this technique, we identify two-quantum microwave absorption and emission processes, unambiguously demonstrating the $S = 3/2$ ground state of V_{Si} (in contrast to the $S = 1$ ground state of the NV defect in diamond). Furthermore, to induce a population inversion, we use relatively weak optical excitation of several hundreds of milliwatts, which is significantly lower than in the case of organic systems. Using this excitation we have achieved steady-state stimulated microwave emission at room temperature. Without an external magnetic field, the emission frequency (ν) corresponds to the zero-field splitting, which ranges from several tens of megahertz to above 1 GHz (ref. 24). By applying an external magnetic field, ν can be tuned over a large spectral range.

The material properties of SiC, including intrinsic defects, have been investigated for decades. In particular, the V_{Si} centres were

[1]Experimental Physics VI, Julius-Maximilian University of Würzburg, 97074 Würzburg, Germany, [2]Ioffe Physical-Technical Institute, 194021 St Petersburg, Russia, [3]Bavarian Center for Applied Energy Research (ZAE Bayern), 97074 Würzburg, Germany. *e-mail: dyakonov@physik.uni-wuerzburg.de

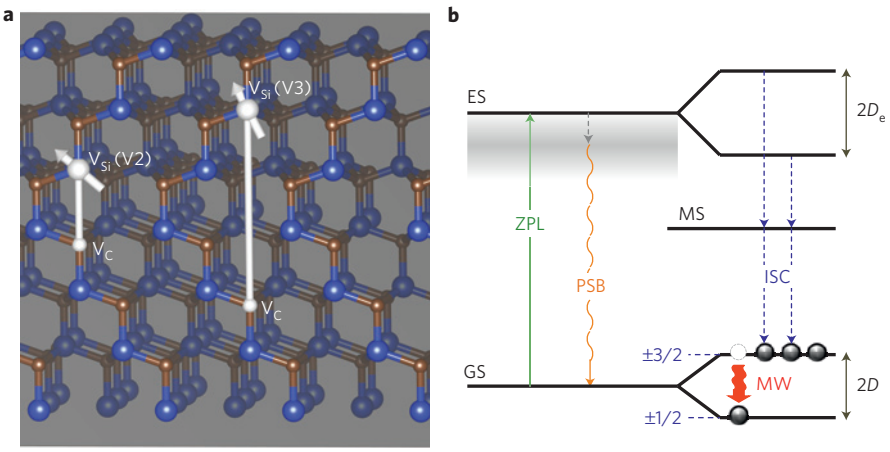

Figure 1 | A model for V_{Si} defects and corresponding Jablonski diagram. a, 6H-SiC lattice in the $(11\bar{2}0)$ plane. V_{Si} is an intrinsic atomic defect, whose spin and optical properties are due to the perturbation along the *c* axis by a carbon vacancy (V_C). **b**, A very sharp optical resonant transition between the ground state (GS) and the excited state (ES) of V_{Si} results in the ZPL. Owing to the interaction with phonons, the phonon sideband (PSB) appears in emission. Alternatively, non-radiative relaxation occurs through the metastable state (MS). Owing to the intersystem crossing (ISC), the higher-lying spin sublevel of the ground state ($m_s = \pm 3/2$) is preferentially populated. Relaxation to the lower-lying ground state spin sublevel ($m_s = \pm 1/2$) results in microwave (MW) emission. 2*D* and $2D_e$ denote the zero-field splitting in the ground singlet state and excited state, respectively.

identified in the 1980s (ref. 18). The ESR experiments on V_{Si} performed about 10 years ago were interpreted in terms of the triplet state ^{3}A (refs 19,20). In these earlier experiments, the V_{Si}-related ESR lines were observed only under optical excitation, and it was suggested that ^{3}A is an excited state, whereas the ground state is a singlet ^{1}A. Recently, in ESR experiments performed in the W-band ($\nu = 95$ GHz), the 'high-spin-related' signal has been detected at a very low temperature in complete darkness[21]. This excludes contribution of excited states and suggests that the V_{Si} ground singlet state is a high-spin state. In the initial interpretation, it was assumed that this ground state is a triplet ^{3}A with $S = 1$. Alternatively, it was also suggested that the V_{Si} defect is negatively charged and its ground state is a quadruplet ^{4}A with $S = 3/2$ (refs 22,23). The challenge in unambiguously distinguishing between these two cases is due to the presence of a large number of different types of defect, whose contributions to the ESR spectra may not be negligible.

To avoid this problem, we use the double radio-optical resonance, which allows us to selectively address only one type of defect[15]. We resonantly excite into the zero-phonon line (ZPL) transition, which is unique for each V_{Si} defect and has an extremely narrow spectral width. Owing to the intersystem crossing, the excited state relaxes through a metastable state, generating an inverse population in the ground state (Fig. 1b). Alternatively, there is a phonon-assisted radiative recombination to the ground state, which forms the phonon sideband (redshifted relative to ZPL) in the photoluminescence spectrum. Remarkably, the radiative recombination rate is different for each spin sublevel, which is a direct consequence of spin-selective intersystem crossing. Resonant microwave absorption or stimulated emission changes the spin population, resulting in a change in the photoluminescence intensity (ΔPL; the modelling of this spin-selective photokinetics[25] is presented in Supplementary Information). The ODMR signal is obtained as $\Delta PL/PL$ at a fixed frequency $\nu = 9.4$ GHz as a function of the magnetic field *B* applied along the *c* axis of SiC.

ODMR

We now present experimental data for the V_{Si} defect attributed to the ZPL labelled as the V2-line in the photoluminescence spectrum of 6H-SiC (ref. 20). We optically excite into the V_{Si}(V2) ZPL with the energy $E_2 = 1.397$ eV and measure the ODMR spectrum (black line in Fig. 2a). It consists of four pairs of resonances, labelled as

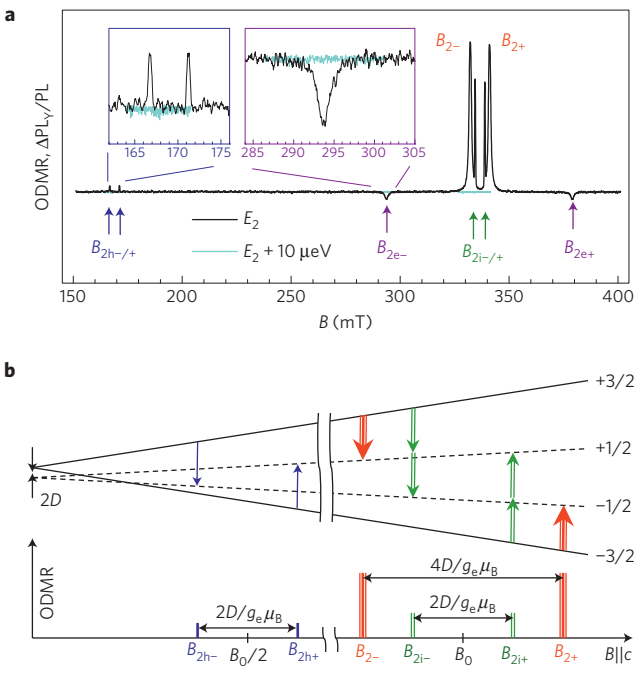

Figure 2 | ODMR fingerprint of V_{Si} defects in SiC. a, ODMR spectra obtained in 6H-SiC under optical excitation with the energy of the V_{Si}(V2) ZPL transition $E_2 = 1.397$ eV and with a slightly detuned energy $E = E_2 + 10\ \mu$eV. $B \| c$ and $\nu = 9.43451$ GHz. **b**, Energy-level diagram of the V_{Si} quadruplet ground state shown as a function of magnetic field and the microwave-induced transitions observed in **a**.

$B_{2\pm}$, $B_{2i\pm}$, $B_{2e\pm}$ and $B_{2h\pm}$. We ascertain that all of these resonances are associated with the V_{Si}(V2) defect—they disappear when the excitation energy is detuned off the V_{Si}(V2) ZPL by only 10 μeV (a few gigahertz; light-coloured flat line in Fig. 2a).

The origin of these resonances is explained in the scheme of Fig. 2b. It is based on the standard spin Hamiltonian, and when the magnetic field is applied along the *c* axis of SiC the energy levels are given by

$$E_{m_s} = g_e \mu_B B m_s + D m_s^2 \quad (1)$$

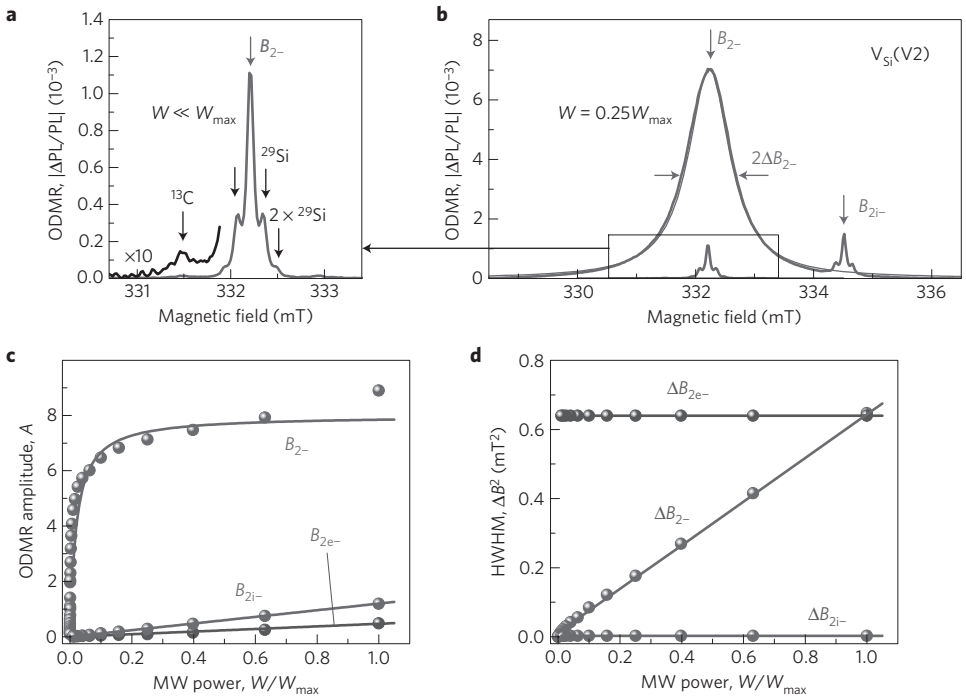

Figure 3 | Microwave power dependence of the V_{Si}(V2) ODMR spectrum. a, Low-power regime, $W = 1.6 \times 10^{-4} W_{max}$. **b**, High-power regime, $W = 0.25 W_{max}$. On the right side of the spectrum one can clearly see one of the two multi-quantum spin resonances with resolved hyperfine structure. A Lorentzian fit of the B_{2-} resonance is represented by the thin line. **c**, Absolute amplitude |ΔPL/PL| of different ODMR resonances as a function of microwave power. **d**, Half-width at half-maximum of different ODMR resonances as a function of microwave power. Solid lines in **c**,**d** are fits within a standard ESR model (see Supplementary Information).

Here, $g_e \approx 2.0$ is the electron g-factor and μ_B is the Bohr magneton. The crystal field D is individual for each type of V_{Si} defect, and m_s is the spin projection of total spin S.

The strongest resonances at $B_{2\pm}$ in Fig. 2a are ascribed to the transitions with $\Delta m_s = \pm 1$. According to equation (1) with $S = 3/2$, the difference in the positions of these resonances corresponds to zero-field splitting $2D_2 = g_e \mu_B (B_{2+} - B_{2-})/2$. We find for V_{Si}(V2) $2D_2 = 0.527$ μeV (127 MHz), in agreement with the earlier reported value[26].

We stress that, on the basis only of the observation of the $\Delta m_s = \pm 1$ resonances, one cannot distinguish between spin $S = 1$ and $S = 3/2$ states. In the $S = 1$ case, two allowed ODMR transitions are also expected. The only difference would be the presence of an additional resonance at the 'central' magnetic field $B_0 = h\nu/g_e\mu_B$ for $S = 3/2$, corresponding to the transition $(-1/2 \rightarrow +1/2)$. However, the amplitude of this resonance can be negligibly small, if the populations of the $m_s = \pm 1/2$ states are equal.

The observation of a half-field resonance at $B_0/2$ is frequently used to identify triplets ($S = 1$) in organic materials[27]. This half-field $\Delta m_s = \pm 2$ resonance corresponds to the transition $(-1 \rightarrow +1)$. In contrast, we observe two resonances around $B_0/2$, at $B_{2h-} = 167$ mT and $B_{2h+} = 171$ mT (Fig. 2a). Remarkably, $B_{2h+} - B_{2h-} = (B_{2+} - B_{2-})/2$ and these resonances are ascribed to the $(+3/2 \rightarrow -1/2)$ and $(-3/2 \rightarrow +1/2)$ transitions, respectively (Fig. 2b). This observation provides strong evidence that V_{Si}(V2) has $S = 3/2$ spin state. This is also in agreement with the magnetic field angular dependence (see Supplementary Information).

We now discuss another pair of resonances, labelled in Fig. 2a as $B_{2i\pm}$. They are located in between the pair of the strongest $B_{2\pm}$ resonances and look like satellites. These inner resonances are observed for different V_{Si} defects, in 6H-SiC as well as in 4H-SiC (see Supplementary Information). In all cases, we obtain the splitting $B_{2i+} - B_{2i-} = B_{2h+} - B_{2h-}$, that is, half of that for $B_{2\pm}$. On the basis of this general property, we ascribe these ODMR lines to the two-quantum spin resonances[28] with $\Delta m_s = \pm 2$, as explained in Fig. 2b.

To further investigate the ODMR fingerprint of V_{Si} defects, we performed microwave power (W) dependence experiments (Fig. 3). The maximum output power provided by our microwave generator is $W_{max} = 2$ W. For $W < 10^{-4} W_{max}$, we observe a narrow resonance at B_{2-} and several satellites due to the hyperfine interaction with nuclear spins of the isotopes ^{29}Si and ^{13}C (Fig. 3a). For high microwave power $W \sim W_{max}$ (Fig. 3b), the B_{2-} resonance broadens and the isotope satellites are no longer resolved. The power dependences are well described within a standard ESR model (see Supplementary Information). Figure 3 also demonstrates a high efficiency of the two-quantum $\Delta m_s = \pm 2$ spin transitions with rising microwave power. The reason for this is the presence of real intermediate states ($m_s = \pm 1/2$), and the probability of this two-quantum process is inversely proportional to the detuning[29] $h\nu - (E_{-1/2(+3/2)} - E_{-3/2(+1/2)})$, which is equal to D according to equation (1).

Finally, we discuss the origin of the $B_{2e\pm}$ resonances in Fig. 2a. Remarkably, they have a different sign compared with the $B_{2\pm}$ resonances, suggesting that the $B_{2e\pm}$ and $B_{2\pm}$ ODMR lines should be associated with different states. On the other hand, by tuning the laser wavelength, we demonstrate that all of the resonances in Fig. 2a should be related to the V_{Si}(V2) defect. We ascribe the $B_{2\pm}$ resonances (and accompanying resonances at $B_{2h\pm}$, $B_{2i\pm}$) to the ground state and the $B_{2e\pm}$ resonances to an excited state of V_{Si}(V2). The significant broadening of the $B_{2e\pm}$ resonances due to a short lifetime in the excited state[30] is also in agreement with this interpretation. Using equation (1), we obtain a value of zero-field splitting in the excited state $2D_{2e} = 10$ μeV (2.42 GHz).

So far, we have presented data for only one type of V_{Si} defect, which is attributed to the characteristic ZPL labelled as V2 in the photoluminescence spectrum. We now turn to another V_{Si} defect, labelled as the V3-line[20]. To measure the corresponding ODMR

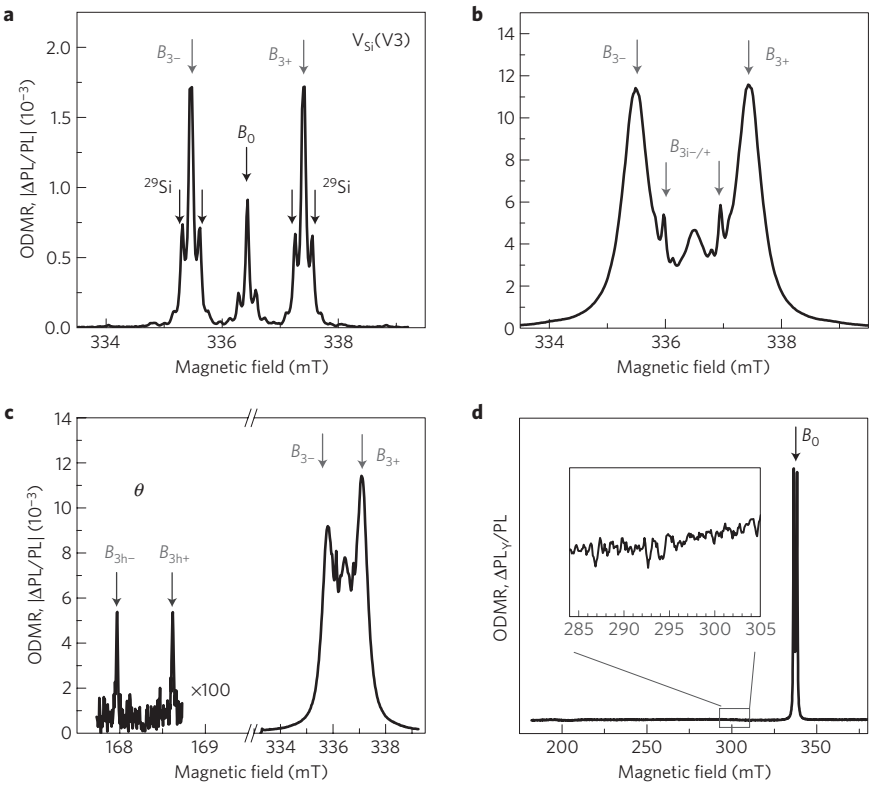

Figure 4 | ODMR spectra obtained under optical excitation with the energy of the V_{Si}(V3) ZPL transition $E_3 = 1.368$ eV. a, Low-power regime, $W = 3 \times 10^{-3} W_{max}$. **b**, High-power regime, $W = W_{max}$. **c**, ODMR spectrum obtained at an angle between the *c* axis and applied magnetic field $\theta = 30°$, indicating the presence of the half-field resonances. **d**, ODMR spectrum recorded in a wide range of magnetic fields, indicating the absence of the outer resonances. The inset shows the magnetic field range where one observes the outer resonance (B_{2e-}) for V_{Si}(V2) (see Fig. 2a).

spectrum (Fig. 4), we tune the laser wavelength in resonance with the V_{Si}(V3) ZPL ($E_3 = 1.368$ eV). In the case of low microwave power, $W = 3 \times 10^{-3} W_{max}$, the ODMR spectrum consists of three narrow resonances and their satellites due to the hyperfine interaction with nuclear $I = 1/2$ spins of the isotope ^{29}Si (Fig. 4a). As for V_{Si}(V2), the resonances at magnetic fields B_{3-} and B_{3+} correspond to the transitions $(+3/2 \rightarrow +1/2)$ and $(-3/2 \rightarrow -1/2)$, respectively (Fig. 2b). The central resonance at B_0 could be ascribed to the $(+1/2 \rightarrow -1/2)$ transition.

With rising microwave power the resonances become broader, and the two-quantum spin resonances at $B_{3i\pm}$ can be observed. We are also able to detect the half-field $\Delta m_s = \pm 2$ transitions $B_{3h\pm}$. They are most pronounced when the magnetic field is applied at an angle $\theta = 30°$ with respect to the *c* axis of 6H-SiC, as shown in Fig. 4c (see also Supplementary Information). Figure 4d shows the V_{Si}(V3) ODMR spectrum in a wide range of magnetic fields. In contrast to V_{Si}(V2), we do not observe outer resonances ascribed to the V_{Si}(V3) excited state (the inset of Fig. 4d). A possible reason for this could be a shorter spin lifetime in the V_{Si}(V3) excited state.

Room-temperature stimulated microwave emission

As depicted in Fig. 1b, a population inversion in the V_{Si} ground singlet state is generated under optical excitation owing to the spin-selective intersystem crossing. First, we demonstrate that this process remains efficient at room temperature. Figure 5a shows an ODMR spectrum obtained at room temperature $T = 300$ K. At high temperatures, the ZPLs are not resolved, and we excite into the phonon-assisted absorption band[15]. Two pairs of resonances are observed, and from the comparison with Figs 2–4, they can clearly be associated with the $\Delta m_s = \pm 1$ transitions of the V_{Si}(V2) and V_{Si}(V3) defects. This is the first time that ODMR is detected for identified spin defects in 6H-SiC at room temperature[14].

A population inversion is a prerequisite for stimulated emission, and we now demonstrate room-temperature steady-state stimulated microwave emission under relatively low optical pumping. As in the case of the above ODMR experiments, the samples are inserted into an X-band cavity ($\nu = 8.9$ GHz), and we perform light-induced ESR measurements using an 808 nm laser with a power of 600 mW. To increase the signal-to-noise ratio at room temperature, we slightly modulate the magnetic field, resulting in the derivative shape of the ESR lines (Fig. 5b). The most pronounced effect is observed for V_{Si}(V3). The ESR signal at B_{3-} is of nearly the same amplitude but inverted relative to the ESR signal at B_{3+}, indicating that microwave emission occurs at one of these magnetic fields. Comparison with the scheme of Fig. 2b unambiguously suggests that this magnetic field is B_{3-}. This is also confirmed by the light-induced ESR experiments performed at a lower temperature $T = 77$ K, where microwave emission and absorption are directly detectable without magnetic field modulation (see Supplementary Information). For V_{Si}(V2) the effect is much weaker but still recognizable—one detects microwave absorption at B_{2+}, whereas the absence of the ESR line at B_{2-} means that the photo-induced spin pumping and spin relaxation processes compensate each other.

Stimulated microwave emission is indispensable to implement a travelling-wave quantum amplifier[31]. Our analysis (see Methods) shows that a very high gain and a low noise temperature can be achieved in SiC quantum amplifiers at a room-temperature environment. Furthermore, for bigger SiC samples, the resonator filling factor is significantly larger than in the present experiments, and the masing effect in SiC should also be achieved.

Discussion and outlook

First, we discuss the origin of the V_{Si}(V2) and V_{Si}(V3) defects. They have spin $S = 3/2$ and should be negatively charged. On the other

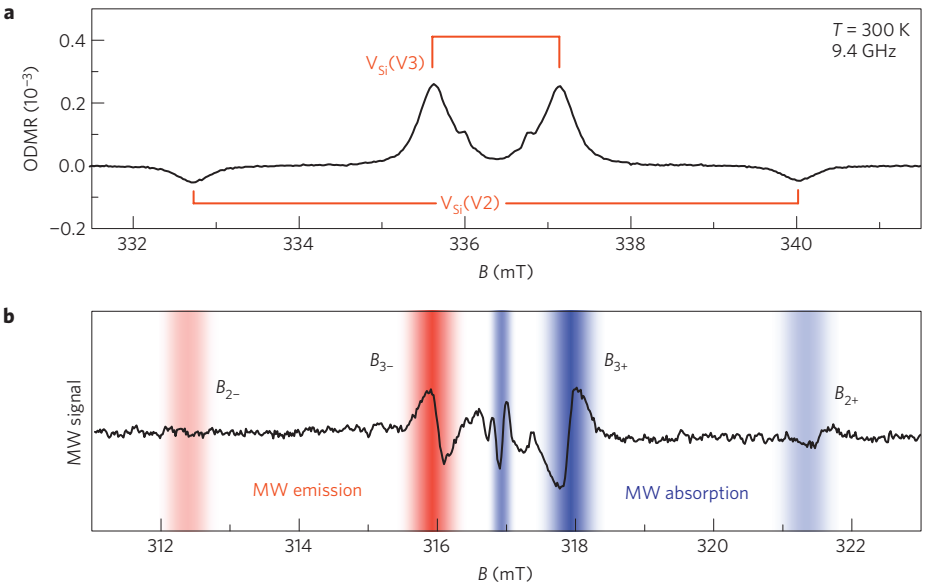

Figure 5 | Room-temperature population inversion of the V_{Si} defects. a, ODMR spectra obtained under optical excitation into the phonon-assisted band with $E = 1.579$ eV (785 nm). **b**, Light-induced (808 nm) stimulated microwave emission and absorption. The derivative shape of the ESR lines is due to the magnetic field modulation.

hand, an isolated negatively charged silicon vacancy is well known to possess a high symmetry, not allowing for zero-field splitting[22]. We suggest a model in which the silicon vacancy is perturbed by another intrinsic defect, probably a carbon vacancy (V_C), located at some distance along the c axis (Fig. 1a). This model is consistent with the observed uniaxial symmetry of V_{Si} (see Supplementary Information). In contrast to the NV defect in diamond[11] and the $(V_{Si}–V_C)^0$ di-vacancy in SiC (ref. 32), V_{Si} and V_C are not chemically bound in our model. Given that about 250 polytypes of SiC are known and that in each several configurations of V_{Si} and V_C are possible, there should exist about 1,000 such V_{Si} defects with unique characteristics.

The properties of the V_{Si} defects can be used for a broad range of quantum applications. The ODMR technique presented in this paper is not limited to ensemble measurements and can be applied to a single defect as well. This makes V_{Si} attractive for use as room-temperature qubits and spin sensors. An interesting property is that a single V_{Si} defect at certain conditions can emit indistinguishable microwave photon pairs owing to the two-quantum process, suggesting a new platform for on-a-chip quantum information processing. Furthermore, the demonstration of steady-state stimulated microwave emission in SiC at room temperature is a crucial step towards fabricating solid-state masers and travelling-wave quantum amplifiers with an extraordinarily low noise level. This can potentially bring long-distance communication, radar and radio location systems to a new level that is unachievable with the present-day technologies.

Methods

Samples. We present experimental results for 6H polytype SiC crystals grown by two different methods. In the case of the Lely method, the V_{Si} defects already exist in the as-grown samples. To generate the V_{Si} defects in the samples grown by the sublimation technique, they have been irradiated with fast neutrons to a dose up to 10^{16} cm^{-2}. Typical V_{Si} concentration is $\sim 10^{15}$ cm^{-3}. All samples show similar behaviour, with the exception that the photo-induced microwave emission in the Lely crystals disappears above 100 K, most probably owing to the ionization of nitrogen donors that are present in Lely SiC as unintentional dopants. We also investigated epitaxial 4H-SiC samples and obtained similar results to those presented here.

Experimental set-up. The ODMR experiments are performed in an X-band cavity ($Q = 3{,}000$, $\nu = 9.4$ GHz) with direct optical access. The samples are mounted in a liquid helium flow cryostat and kept at constant temperature $T = 4$ K. We use a tunable diode laser system (linewidth below 1 MHz) to resonantly excite into the ZPL transition. The laser is focused onto the sample to a power density about 1 W cm^{-2}. The photoluminescence is passed through a 900 or 950 nm long-pass filter and detected by a fast Si photodiode. We chop the microwave radiation, and the output signal at the photodiode is locked-in. We denote the in-phase and quadrature components as ΔPL_X and ΔPL_Y, respectively. The ODMR signal is obtained as a normalized change in photoluminescence ($\Delta PL/PL$) of the the phonon sideband with $\Delta PL = \sqrt{(\Delta PL_X)^2 + (\Delta PL_Y)^2}$. Where not indicated otherwise, the magnetic field is applied parallel to the c axis of 6H-SiC.

The photo-induced microwave emission is measured in a commercial X-band spectrometer ($\nu = 8.9$ GHz) at nominal microwave power of 10 mW. A diode laser operating at 808 nm is used to excite all types of V_{Si} defect through phonon-assisted absorption at room temperature. The unfocused laser beam illuminates the whole sample (typical area of a few square millimetres) providing a power density of about 3 W cm^{-2}.

Gain and noise temperature. Here, we use the same approach that was successfully applied for the maser amplifiers based on paramagnetic centres in ruby (which also have four spin sublevels in the ground state)[31], but with the parameters of the V_{Si} defects in SiC. Owing to stimulated emission, the intensity of the propagating microwave radiation increases exponentially. This increase can be described by the imaginary part of the magnetic susceptibility χ''. It depends on the Einstein coefficients as well as on the degree of the population inversion $\rho < 0$, and can be brought to the form

$$\chi'' \approx 10^{-13} \rho N_V \frac{\sigma^2}{\Delta\nu}$$

Here, N_V is the V_{Si} concentration in cm^{-3}, and $\Delta\nu$ is the spectral width of the corresponding ESR resonance in hertz. In the case of pure spin states, the effective matrix element is $\sigma^2 = 1/2$. The interaction between a SiC crystal and the microwave field within the cavity is characterized by the magnetic decrement

$$d_m = 4\pi|\chi''|\eta$$

where η is the filling factor of the resonator.

From the comparison of the ESR spectra, recorded in the dark and under optical pumping, one estimates[17] $|\rho| > 0.8$. Using other parameters from our experiments, that is, $N_V = 10^{15}$ cm^{-3}, $\Delta\nu = 5 \times 10^6$ Hz and $\eta = 3 \times 10^{-4}$, one obtains $d_m = 3 \times 10^{-8}$. The gain factor can be calculated using

$$G = \left(\frac{2d_m}{1 + d_m \nu / \Delta\nu} Q + 1 \right)^2$$

which gives $G = 1.0003$. Such a low value of G probably does not exceed losses in the cavity, resulting in overall microwave absorption in our experiments. However, the gain can be increased by using a larger crystal (such that $\eta \simeq 1$) with a higher

V_{Si} concentration ($N_V = 10^{18}$ cm^{-3}). In this case $d_m = 0.1$ and expected gain is $G = 7$ (or $G_{dB} = 8$ dB).

Much higher gain can be achieved in travelling-wave quantum amplifiers, for which

$$G_{dB} = 27.3 \frac{c}{v_g} \frac{l}{\lambda} d_m - L_{dB}$$

Here, v_g is the group (travelling) velocity, and the ratio $c/v_g = 2.55$ is given by the dielectric constant of SiC. To estimate the gain, we assume that the crystal length (l) is equal to the microwave wavelength ($\lambda = 3$ cm at $\nu = 9$ GHz), and we take losses on a level of 50% ($L_{dB} = 3$). With these parameters we obtain $G_{dB} = 4$ dB. The group velocity can be significantly reduced using systems with frequency dispersion, and the ratio $c/v_g = 50$ can be achieved[31], providing $G_{dB} > 100$ dB.

Intrinsic noise of a quantum amplifier is caused by spontaneous emission and can be characterized by the effective noise temperature ($T_{noise} \approx h\nu/k_B$), which is $T_{noise} = 0.4$ K at $\nu = 9$ GHz. In addition to that, the noise of the microwave guide should be considered. It could be much smaller than the environment temperature (T), if the number of microwave emitters is much larger then the number of thermally excited microwave photons. One can approximate for the total noise temperature

$$T_{noise} \approx \frac{h\nu}{k_B} \frac{G_{dB} + L_{dB}}{G_{dB}} + T \frac{L_{dB}}{G_{dB}}$$

At ambient conditions ($T = 300$ K) this still gives a very small value $T_{noise} \approx 10$ K. For comparison, the typical noise temperatures of ruby masers are in the range from 2 to 25 K (ref. 6).

Received 7 February 2013; accepted 31 October 2013; published online 8 December 2013

References

1. O'Brien, J. L., Furusawa, A. & Vučković, J. Photonic quantum technologies. *Nature Photon.* **3,** 687–695 (2009).
2. Santori, C., Fattal, D. & Yamamoto, Y. *Single-Photon Devices and Applications* (Wiley-VCH, 2010).
3. Houck, A. A. *et al.* Generating single microwave photons in a circuit. *Nature* **449,** 328–331 (2007).
4. Astafiev, O. *et al.* Single artificial-atom lasing. *Nature* **449,** 588–590 (2007).
5. Bozyigit, D. *et al.* Antibunching of microwave-frequency photons observed in correlation measurements using linear detectors. *Nature Phys.* **7,** 154–158 (2010).
6. Clauss, R. C. & Shell, J. S. *Low-Noise Systems in the Deep Space Network* (Jet Propulsion Laboratory California Institute of Technology, 2008).
7. Yarmus, L., Rosenthal, J. & Chopp, M. EPR of triplet excitons in tetracene crystals: Spin polarization and the role of singlet exciton fission. *Chem. Phys. Lett.* **16,** 477–481 (1972).
8. Agostini, G., Corvaja, C., Giacometti, G. & Pasimeni, L. Optical, zero-field ODMR and EPR studies of the triplet states from singlet fission in biphenyl-TCNQ and biphenyl-tetrafluoro-TCNQ charge-transfer crystals. *Chem. Phys.* **173,** 177–186 (1993).
9. Koptyug, I. V., Goloshevsky, A. G., Zavarine, I. S., Turro, N. J. & Krusic, P. J. CIDEP studies of fullerene-derived radical adducts. *J. Phys. Chem. A* **104,** 5726–5731 (2000).
10. Oxborrow, M., Breeze, J. D. & Alford, N. M. Room-temperature solid-state maser. *Nature* **488,** 353–356 (2012).
11. Jelezko, F. & Wrachtrup, J. Single defect centres in diamond: A review. *Phys. Status Solidi a* **203,** 3207–3225 (2006).
12. Harrison, J., Sellars, M. J. & Manson, N. B. Optical spin polarization of the N–V centre in diamond. *J. Lumin.* **107,** 245–248 (2004).
13. Baranov, P. *et al.* Silicon vacancy in SiC as a promising quantum system for single-defect and single-photon spectroscopy. *Phys. Rev. B* **83,** 125203 (2011).
14. Koehl, W. F., Buckley, B. B., Heremans, F. J., Calusine, G. & Awschalom, D. D. Room temperature coherent control of defect spin qubits in silicon carbide. *Nature* **479,** 84–87 (2011).
15. Riedel, D. *et al.* Resonant addressing and manipulation of silicon vacancy qubits in silicon carbide. *Phys. Rev. Lett.* **109,** 226402 (2012).
16. Fuchs, F. *et al.* Silicon carbide light-emitting diode as a prospective room temperature source for single photons. *Sci. Rep.* **3,** 1637 (2013).
17. Soltamov, V., Soltamova, A., Baranov, P. & Proskuryakov, I. Room temperature coherent spin alignment of silicon vacancies in 4H- and 6H-SiC. *Phys. Rev. Lett.* **108,** 226402 (2012).
18. Vainer, V. S. & Il'in, V. A. Electron spin resonance of exchange-coupled vacancy pairs in hexagonal silicon carbide. *Sov. Phys. Solid State* **23,** 2126–2133 (1981).
19. Sörman, E. *et al.* Silicon vacancy related defect in 4H and 6H SiC. *Phys. Rev. B* **61,** 2613–2620 (2000).
20. Wagner, M. *et al.* Electronic structure of the neutral silicon vacancy in 4H and 6H SiC. *Phys. Rev. B* **62,** 16555–16560 (2000).
21. Orlinski, S., Schmidt, J., Mokhov, E. & Baranov, P. Silicon and carbon vacancies in neutron-irradiated SiC: A high-field electron paramagnetic resonance study. *Phys. Rev. B* **67,** 125207 (2003).
22. Wimbauer, T., Meyer, B., Hofstaetter, A., Scharmann, A. & Overhof, H. Negatively charged Si vacancy in 4H SiC: A comparison between theory and experiment. *Phys. Rev. B* **56,** 7384–7388 (1997).
23. Mizuochi, N. *et al.* Continuous-wave and pulsed EPR study of the negatively charged silicon vacancy with $S = 3/2$ and C_{3v} symmetry in n-type 4H-SiC. *Phys. Rev. B* **66,** 235202 (2002).
24. Falk, A. L. *et al.* Polytype control of spin qubits in silicon carbide. *Nature Commun.* **4,** 1819 (2013).
25. Nizovtsev, A. P. *et al.* Spin-selective low temperature spectroscopy on single molecules with a triplet–triplet optical transition: Application to the NV defect centre in diamond. *Opt. Spectrosc.* **94,** 848–858 (2003).
26. von Bardeleben, H., Cantin, J., Vickridge, I. & Battistig, G. Proton-implantation-induced defects in n-type 6H- and 4H-SiC: An electron paramagnetic resonance study. *Phys. Rev. B* **62,** 10126–10134 (2000).
27. De Ceuster, J., Goovaerts, E., Bouwen, A. & Dyakonov, V. Recombination of triplet excitons and polaron pairs in a derived paraphenylene vinylene pentamer. *Phys. Rev. B* **68,** 125202 (2003).
28. Baranov, P. G., Romanov, N. G., Khramtsov, V. A. & Vikhnin, V. S. Oriented silver chloride microcrystals and nanocrystals embedded in a crystalline KCl matrix, as studied by means of electron paramagnetic resonance and optically detected magnetic resonance. *J. Phys. Condens. Matter* **13,** 2651–2669 (2001).
29. Hughes, V. & Geiger, J. Two-quantum transitions in the microwave Zeeman spectrum of atomic oxygen. *Phys. Rev.* **99,** 1842–1845 (1955).
30. Fuchs, G. *et al.* Excited-state spectroscopy using single spin manipulation in diamond. *Phys. Rev. Lett.* **101,** 117601 (2008).
31. Kornienko, L. S. & Shteinshleiger, V. B. Quantum amplifiers and their application in space research. *Sov. Phys. Usp.* **21,** 852–864 (1978).
32. Baranov, P. G. *et al.* EPR identification of the triplet ground state and photoinduced population inversion for a Si–C divacancy in silicon carbide. *J. Exp. Theor. Phys. Lett.* **82,** 441–443 (2005).

Acknowledgements

This work has been supported by the Bavarian Ministry of Economic Affairs, Infrastructure, Transport and Technology, Germany as well as by the Ministry of Education and Science, Russia under agreements No. 8017, No. 8568, grant of the President 14.122.13.6053-MK, Russia, the Programs of the Russian Academy of Sciences: 'Spintronics' and 'Fundamentals of nanostructure and nanomaterial technologies' and by the RFBR No. 13-02-00821. We thank V. A. Ilyin and E. N. Mokhov for fruitful discussions as well as M. Heiber for careful reading of our manuscript and useful suggestions.

Author contributions

H.K., V.A.S., D.R., S.V. and F.F. conducted the experiments; P.G.B., V.A.S., D.R. and G.V.A. analysed the experimental data; A.S., P.G.B., V.D. and G.V.A. conceived the experiments; G.V.A. wrote the main manuscript text; V.D. critically reviewed and corrected the manuscript; all authors discussed the results.

Additional information

Supplementary information is available in the online version of the paper. Reprints and permissions information is available online at www.nature.com/reprints. Correspondence and requests for materials should be addressed to V.D.

Competing financial interests

The authors declare no competing financial interests.